ARTICLES

Journal of Semiconductors
(2020) 41, 072903
doi: 10.1088/1674-4926/41/7/072903

Mn doping effects on the gate-tunable transport properties of Cd_3As_2 films epitaxied on GaAs

Hailong Wang[1, 2], Jialin Ma[1, 2], Qiqi Wei[1, 2], and Jianhua Zhao[1, 2, 3, †]

[1]State Key Laboratory of Superlattices and Microstructures, Institute of Semiconductors, Chinese Academy of Sciences, Beijing 100083, China

[2]Center of Materials Science and Optoelectronics Engineering & CAS Center for Excellence in Topological Quantum Computation, University of Chinese Academy of Sciences, Beijing 100190, China

[3]Beijing Academy of Quantum Information Sciences, Beijing 100193, China

Abstract: The Mn doping effects on the gate-tunable transport properties of topological Dirac semimetal Cd_3As_2 films have been investigated. Mn-doped Cd_3As_2 films are directly grown on GaAs(111)B substrates by molecular-beam epitaxy, during which the single crystal phase can be obtained with Mn concentration less than 2%. Shubnikov-de Haas oscillation and quantum Hall effect are observed at low temperatures, and electrons are found to be the dominant carrier in the whole temperature range. Higher Mn content results in smaller lattice constant, lower electron mobility and larger effective band gap, while the carrier density seems to be unaffected by Mn-doping. Gating experiments show that Shubnikov-de Haas oscillation and quantum Hall effect are slightly modulated by electric field, which can be explained by the variation of electron density. Our results provide useful information for understanding the magnetic element doping effects on the transport properties of Cd_3As_2 films.

Key words: molecular-beam epitaxy; Dirac semimetal; Cd_3As_2 film; Mn doping; quantum transport

Citation: H L Wang, J L Ma, Q Q Wei, and J H Zhao, Mn doping effects on the gate-tunable transport properties of Cd_3As_2 films epitaxied on GaAs[J]. *J. Semicond.*, 2020, 41(7), 072903. http://doi.org/10.1088/1674-4926/41/7/072903

1. Introduction

As a representative material of topological Dirac semimetal (TDS), Cd_3As_2 has been intensively studied in recent years thanks to its stability in air and its high carrier mobility[1–9]. Following theoretical prediction in 2013, its topological nature was quickly verified by angle-resolved photoemission spectroscopy (ARPES) and quantum transport experiments[1–19]. Novel physical phenomena were also identified, revealing its distinct topological properties[5–30]. For instance, negative magnetoresistance induced by chiral anomaly, 3D quantum Hall effect (QHE), Aharonov-Bohm oscillation, Fano interference, magnetic and superconductive proximity effect have all been demonstrated[12–30]. Cd_3As_2 is also a promising material for potential applications in functional devices because of its enhanced thermoelectric parameters, ultrafast optical dynamics, and robust mid-infrared properties[31–34]. Moreover, Cd_3As_2 plays an important role in the investigation of topological phase transition, in which space inversion and/or time reversal symmetry breaking are critical factors[1, 35–38].

Efficient methods to break the symmetry include introducing strain through lattice mismatch or piezo-electric substrate, or by doping magnetic elements[1]. Theoretically, using first principle calculation based on density functional theory, the electronic and magnetic properties of 3d transition-metal element (3d-TM) doped Cd_3As_2 have been studied, and Cr-doped Cd_3As_2 has been predicted to be a potential room temperature ferromagnetic semiconductor via Monte Carlo simulations[38]. It is also found that 3d-TM doping lowers the symmetry, leading to massive Dirac fermions with an opening gap[33, 38–42]. So far, the band gap opening has been suggested by experiments on the Cr and Mn doped Cd_3As_2 bulk materials and films[33, 39–42]. In addition, magnetic elements would be very important for the transport properties of topological materials because they are usually related to exotic states like quantum anomalous Hall effect or tunable magnetism[33, 38–42].

In this work, we investigate the symmetry breaking effects on the transport properties of Cd_3As_2 films by introducing lattice strain and magnetic element doping. Specifically, Mn-doped Cd_3As_2 films are directly grown on semi-insulating GaAs(111)B substrates by low temperature molecular-beam epitaxy (LT-MBE). Mn concentration higher than 2% would easily cause the generation of second phase, which might be attributed to the large lattice mismatch between GaAs and Cd_3As_2. Shubnikov-de Haas (SdH) oscillation and quantum Hall effect are observed at low temperatures, and electrons are found to be the dominant carrier, both at room temperature and low temperature. Larger Mn content leads to smaller lattice constant, lower electron mobility, and larger effective band gap, while the electron density seems to be unaffected by Mn-doping. Gating experiments show that SdH oscillation and QHE can be slightly modulated by electric field, which is ascribed to the variation of carrier density. Our results are valuable for the study of the magnetic element doping effects on the physical properties of Cd_3As_2 films.

Correspondence to: J H Zhao, jhzhao@semi.ac.cn
Received 29 MARCH 2020; Revised 22 APRIL 2020.

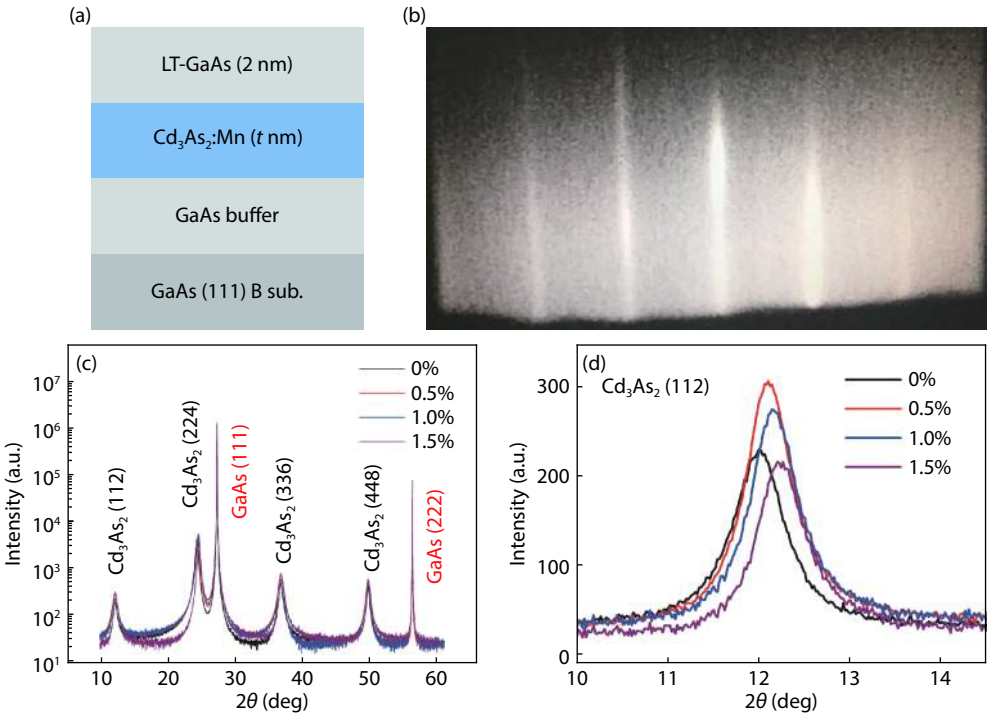

Fig. 1. (Color online) (a) Layer structure, (b) RHEED pattern, and (c) XRD curves of Cd_3As_2 films with various Mn doping concentration. (d) The enlarged XRD curves of (c) around the Cd_3As_2 (112) diffraction peak.

2. Epitaxial growth of Mn-doped Cd_3As_2 films

A series of Cd_3As_2 films with different Mn doping concentration were grown on epi-ready GaAs(111)B substrates, during which the molecular beams of Cd, Mn and As were separately controlled by using three isolated effusion cells. The GaAs buffer layer was deposited at high temperature (560 °C), and the following Mn-doped Cd_3As_2 films and GaAs capping layer (for the aim of avoiding oxidation of Cd_3As_2) was grown at low temperature (180 °C). The growth process was monitored by reflection high-energy electron diffraction (RHEED), and streaky patterns of Cd_3As_2 films could be observed and used to infer the orientation of the crystal plane, as shown in Fig. 1(b). The growth window of Cd_3As_2 films is quite narrow, with the growth temperature in the range from 170 to 200 °C and nominal Cd/As ratio of 0.7 to 3.5. The incorporation of Mn does not obviously affect the growth conditions, and no signature of second phase would appear if the Mn content is less than 2%. When the thickness of the Mn-doped Cd_3As_2 film exceeds 150 nm, the brightness of the RHEED patterns would gradually weaken. Therefore, we will focus on the samples with thickness ranging from 10 to 100 nm, and only the samples with good crystal quality as judged by their XRD and RHEED data will be selected for further investigations. Notice the atoms in Cd_3As_2 (112) arrange themselves in the form of a quasi-hexagon, which explains the epitaxial mode of Cd_3As_2 (112) // GaAs (111) since the GaAs {111} planes are hexagonal as well[2]. This quasi-hexagonal {112} planes are also the largest facet that naturally forms during bulk material growth, implying the lowest surface energy of this special crystal planes[2, 8].

It should be mentioned that the RHEED patterns have a clear change during the transition from GaAs (111) to Cd_3As_2 (112) (corresponding to the process for depositing ~1 nm thick Cd_3As_2), and then kept nearly the same. This suggests a rapid relaxation of Cd_3As_2 lattices, although the lattice mismatch between Cd_3As_2 and GaAs is quite large.

Fig. 1(c) shows the X-ray diffraction (XRD) results of Cd_3As_2 films (50 nm) with Mn doping concentration of 0%, 0.5%, 1.0% and 1.5%, respectively. In the diffraction angles (2θ) range of 10° to 60°, four peaks corresponding to the Cd_3As_2 (112), (224), (336) and (448) crystal planes could also be identified, in addition to the strong GaAs (111) and (222) diffraction peaks. The calculated lattice constants from XRD results are similar with the bulk values, confirming the quick relaxation of the Cd_3As_2 films. This is similar to the results of Cd_3As_2 films grown on GaSb (111) or CdTe buffer layer by LT-MBE, where the lattice mismatch is also not negligible[35, 43–45]. No other peaks are observed with 2θ up to 90° (not shown), implying the high crystal quality of these samples. The Cd_3As_2 diffraction peaks shift slightly to larger angles as the Mn concentration increases as shown in Fig. 1(d), which is probably due to the (partial) incorporation of the Mn atoms into the lattice of Cd_3As_2.

3. Transport properties of Mn-doped Cd_3As_2 films

The Cd_3As_2 samples were fabricated into top-gated field-effect devices, the structure is schematically shown in Fig. 2(a). After the 30 μm wide Hall bar was defined with Cd_3As_2 as the channel via optical lithography and ion-beam milling, a 50 nm thick Al_2O_3 insulating layer was deposited onto the sample at 80 °C by atomic layer deposition (ALD). Finally, an Au/Cr electrode was formed using thermal evaporation and lift-off processes. The electric current was applied along the GaAs [11-2] direction, and the distance between nearby electrodes is 30 μm. To efficiently modulate the transport properties by electric field, relatively thin Cd_3As_2 films (20 nm) were chosen. Temperature dependence of the longit-

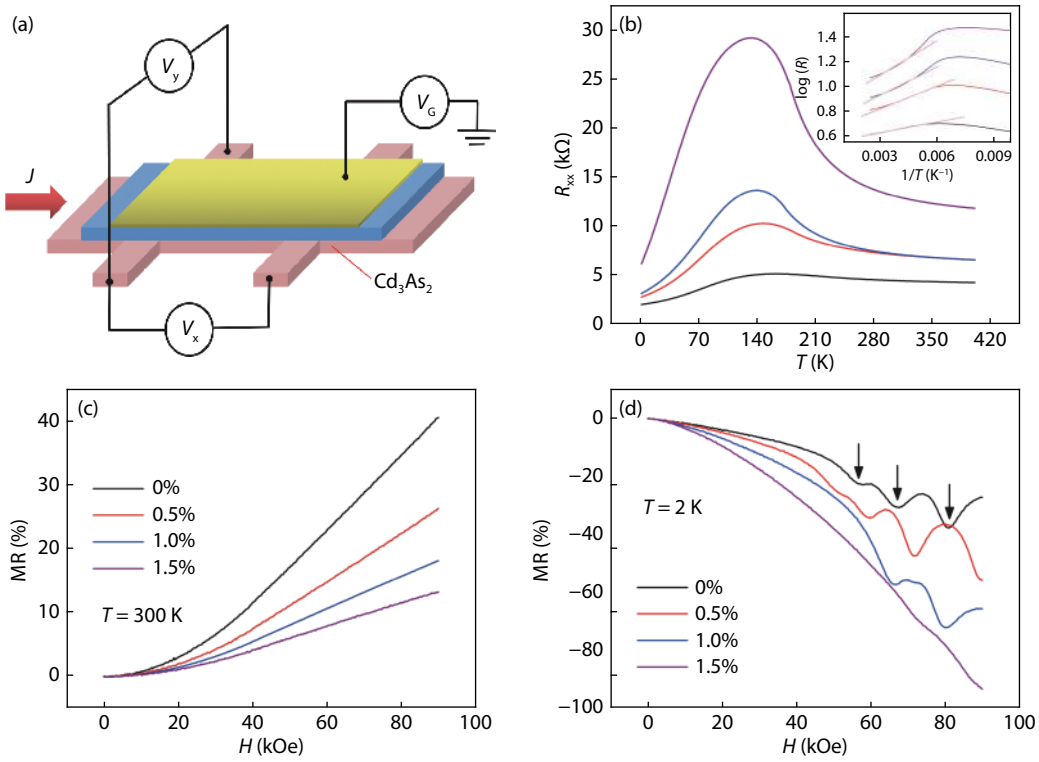

Fig. 2. (Color online) (a) Field effect device diagram, (b) Temperature dependence, and (c, d) Magnetic field dependence of Mn-doped Cd_3As_2 films. The inset of (b) shows the fitting line based on Arrhenius equation, in which the blue curve is offset for clarity.

udinal resistance curves (R_{xx}–T) without applying magnetic field are plotted in Fig. 2(b). Clearly, the four samples with different Mn doping concentration all exhibit semiconductor-like temperature dependency at high temperatures, consistent with the theoretical prediction and previous experimental reports of Cd_3As_2 films grown by MBE[1, 35]. By fitting the R_{xx}–T curve at high temperature region with the following Arrhenius equation:

$$\rho = A\exp\left(E_a/k_BT\right),$$

where E_a and k_B are the activation energy and Boltzmann constant, respectively. The activation energy can be extrapolated, as shown in the inset of Fig. 2(b)[35, 36]. The effective band gap $E_g = E_a/2$ is then estimated to be ~39.2 (57.6, 88.5, 116.7) meV for the 0% (0.5%, 1.0%, 1.5%) Mn-doped sample. Apparently, the larger induced band gap corresponds to higher Mn concentration, while the residual strain might be the main reason for the opening-gap in the case of the non-doped sample[1]. It is interesting that R_{xx} rapidly decreases in the low temperature range, which deviates the low temperature trends as expected for the narrow band gap semiconductors. Although this kind of temperature dependence is also found in some Cd_3As_2 bulk materials, these two cases are not the same due to their different band structures[9]. We will show later that the main reason for the rapid decrease of resistance is the quickly increasing carrier mobility.

The magnetoresistance (MR) curves at 300 K with magnetic field (B) perpendicular to the plane are presented in Fig. 2(c). For this geometric configuration, the positive MR at room temperature changes as a parabolic curve in the low magnetic field region (B < ~4 T), and shows linear dependence in the high magnetic field region. This is quite different from the results of undoped bulk materials, in which linear MR dominates in a large magnetic field range (up to 14.5 T) at high temperatures[8, 9]. Even at low temperatures where the SdH oscillation appears with strong magnetic field, the MR is also linear in the low magnetic field range[8, 9]. The parabolic MR is commonly seen in a variety of semiconductors, and the linear MR might have the same physical origin as the bulk materials[9].

When the temperature was lowered down to 2 K, clear SdH oscillation can be observed for all the samples except the 2% Mn-doped one, as shown in Fig. 2(d). In contrast to the positive MR at 300 K, the MR at 2 K is negative for all the four samples. The amplitude of the SdH oscillations decreases with increasing the Mn concentration, which is an indication of the decreasing electron mobility due to the enhanced magnetic scattering. This result is very different from the previous reports on Cd_3As_2 films with thickness of 100 nm, in which the gap opening effect was thought to be insignificant[39]. This negative MR is probably induced by the enhanced magnetic correlation as the temperature is lowered, which prevails the positive MR. By analyzing the oscillating period $\Delta(1/B)$, the sheet carrier density is determined to be 9.8 (8.5 and 11.2) × 10^{11} cm^{-2} for the 0% (0.5% and 1.0%) Mn-doped sample.

In Fig. 3(a), the Hall resistance as a function of magnetic field (R_{xy}–B) at 300 K is presented. As can be seen from the negative slope in the whole magnetic field range, the transport behavior is mainly determined by electron. We notice that two-carrier transport was reported for Cd_3As_2 films with thickness larger than 50 nm and ~350 nm thick nanoplates, where the Hall resistance was curved due to the competing contributions of electrons and holes[35, 36, 39]. The surface pinning effect in our thin film samples might account for the one carrier dominant transport behavior. Based on the Hall data, the

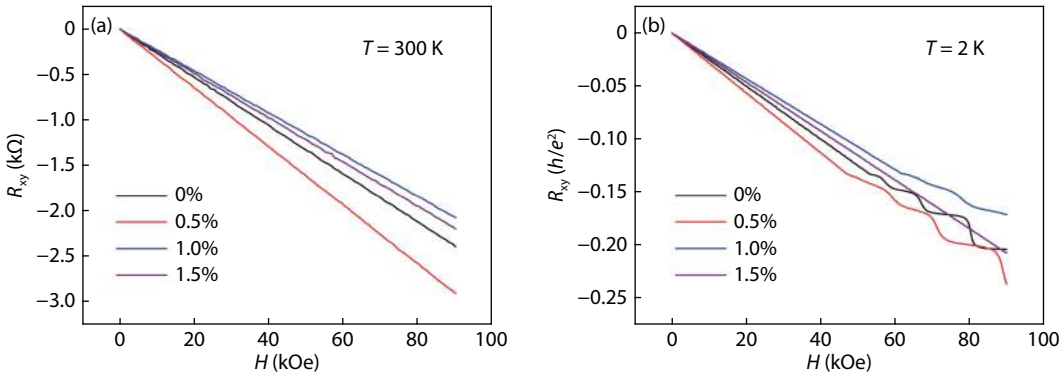

Fig. 3. (Color online) Hall resistance as a function of magnetic field in Mn-doped Cd_3As_2 films at (a) 300 K and (b) 2 K. The unit of (b) is h/e^2 (or ~25812.8 Ω).

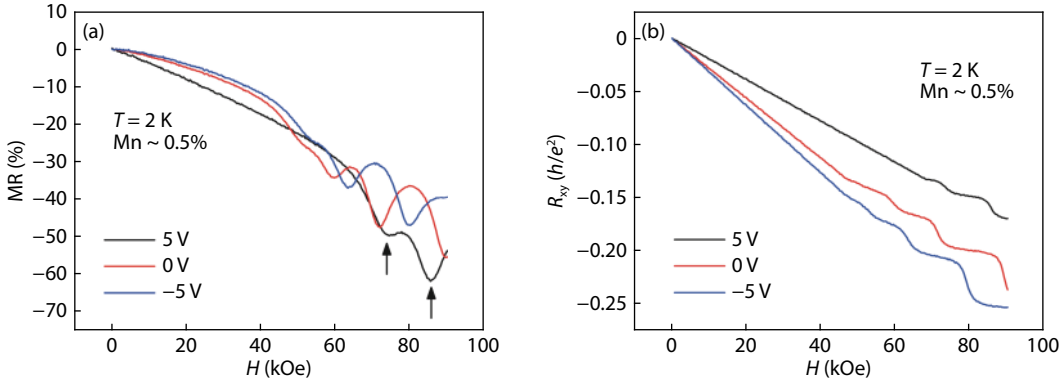

Fig. 4. (Color online) Magnetic field dependence of (a) longitudinal and (b) transverse resistances for a 0.5% Mn-doped Cd_3As_2 film at 2 K.

sheet electron density is calculated to be 23.5 (19.3, 27.1 and 25.6) × 10^{11} cm^{-2}, and the electron mobility of 633 (495, 354 and 207) $cm^2/(V{\cdot}s)$ can also be derived by combining the longitudinal and transverse resistance data together.

Fig. 3(b) shows the R_{xy}–B at 2 K, in which QHE was observed in non-doped and moderately Mn-doped Cd_3As_2 films. Similarly, the negative slope in the low field region gives the sheet electron density of 9.7 (8.6, 11.3 and 10.5) ×10^{11} cm^{-2} for the 0% (0.5%, 1.0% and 1.5%) Mn-doped sample, consistent with the results derived from the SdH oscillation. The electron density at 2 K is several times smaller than that at 300 K, which can be explained by the thermal excitation of carriers. The electron mobility is 3267 (2659, 1785 and 972) $cm^2/(V{\cdot}s)$, about 5.2 (5.4, 5.0 and 4.7) times larger than the room temperature values. The mobility is much lower than the bulk case, but is comparable with films grown on CdTe/mica or GaSb/GaAs substrates[16, 35] Actually, the relatively low mobility also makes the transition region (corresponding to the peak of SdH oscillation) between nearby plateaus not so abrupt. The filling factor at 9 T is $g = 5$, mainly because of the relatively low carrier density. Another two QHE plateaus with $g = 6$ and 7 are also observable, and the $g = 1$ quantum state needs much stronger magnetic field (~40 T). Obviously, the carrier mobility depends on the Mn-doping concentration significantly, since Mn introduces magnetic scattering that decreases the carrier mobility. The carrier density seems to be independent of the Mn doping concentration, suggesting that the incorporation of Mn into the Cd_3As_2 lattice does not introduce extra carriers. Furthermore, we do not observe the signature of anomalous Hall effect (AHE) in our samples, implying the absence of long-range magnetic order in spite of the enhanced magnetic correlation at low temperature, in line with the theoretical calculations[38].

4. Electric-field modulation of the transport properties

Because of the narrow band gap and small density of states at the conduction and valence band edges, it should be relatively easy to shift Fermi energy and thus affect the carrier density. Therefore, we employ the electric field to manipulate the transport properties of the Mn-doped Cd_3As_2 films, and the main results are shown in Fig. 4. The gate voltage is applied by a Keithley 2400 source-meter, whose polarity is defined with respect to the channel.

Fig. 4(a) shows the MR curves of the 0.5% Mn-doped sample modulated by gate voltages at 2 K, from which slight shifts of the SdH oscillation peaks can be identified. Electrons will be accumulated inside the Cd_3As_2 films by applying positive voltage, and depleted by negative gate voltage. The change of sheet electron density could be calculated by $\Delta n_s = \varepsilon_0\varepsilon\Delta E_G/e$, where ε_0, ε, e and ΔE_G are the electric constant, relative electric permittivity (~7 for Al_2O_3), the elementary charge and changing amount of gate electric field, respectively. The variation of electron density leads to a corresponding change of the SdH oscillation, as the period is characterized by its inverse in the form of $\Delta(1/B) = 2e/(\hbar n_s)$, where h is the Planck constant. According to this equation, a positive (negative) gate voltage of 5 V would change the period of

0.056 T^{-1} to 0.0051 (0.0080) T^{-1}. The corresponding values obtained from the experimental data are 0.039 T^{-1} and 0.063 T^{-1} under positive and negative gate voltages, which do not change too much compared with the above estimation. Usually, this large inconsistency is caused by the high-density interface states, which screen the gate electric field from penetrating the Cd_3As_2 films. In our case, the screening is mainly caused by the interface between GaAs and Cd_3As_2, since our previous works on GaAs/(Ga,Mn)As show that the surface states of GaAs capping layer facing to the Al_2O_3 layer can be ignored[46, 47]. The screening effect might be suppressed by using a Cd_3As_2 structure without GaAs layer, which is the topic of further research.

The corresponding change of the Hall resistance is plotted in Fig. 4(b), and the QHE plateau shifts when the gate voltage is varied from 5 to –5 V. Again, the electron density deduced from the slope of the low field data is consistent with the one determined by the SdH oscillation, verifying the gating effect in this sample.

5. Conclusion

In conclusion, by introducing lattice strain and magnetic element doping, we investigate the symmetry breaking effects on the transport properties of Mn-doped Cd_3As_2 films grown on semi-insulating GaAs(111)B substrate. Larger Mn content results in a smaller lattice constant, lower electron mobility, and larger effective band gap, while the electron density seems to be independent of the Mn-doping concentration. Gating experiments show that SdH oscillation and QHE can be slightly modulated by electric field, which is ascribed to the variation of carrier density. Our results are valuable for the study of the magnetic elements doping effects on the physical properties of Cd_3As_2 films.

Acknowledgements

This work is supported by NSFC (Grants Nos. U1632264 and 11704374), and the the Strategic Priority Research Program of the Chinese Academy of Sciences (Grant Nos. XDB44000000 and QYZDY-SSW-JSC015).

References

[1] Wang Z J, Weng H M, Wu Q S, et al. Three-dimensional Dirac semimetal and quantum transport in Cd_3As_2. Phys Rev B, 2013, 88, 125427

[2] Ali M N, Gibson Q, Jeon S, et al. The crystal and electronic structures of Cd_3As_2, the three-dimensional electronic analogue of graphene. Inorg Chem, 2014, 53, 4062

[3] Borisenko S, Gibson Q, Evtushinsky D, et al. Experimental realization of a three-dimensional Dirac semimetal. Phys Rev Lett, 2014, 113, 027603

[4] Liu Z K, Jiang J, Zhou B, et al. A stable three-dimensional topological Dirac semimetal Cd_3As_2. Nat Mater, 2014, 13, 677

[5] Jeon S, Zhou B B, Gyenis A, et al. Landau quantization and quasiparical interference in the three-dimensional Dirac semimetal Cd_3As_2. Nat Mater, 2014, 13, 851

[6] Neupane M, Xu S Y, Sankar R, et al. Observation of a three-dimensional topological Dirac semimetal phase in high-mobility Cd_3As_2. Nat Commun, 2014, 5, 3786

[7] Potter A C, Kimchi I, Vishwanath A. Quantum oscillations from surface Fermi arcs in Weyl and Dirac semimetals. Nat Commun, 2014, 5, 5161

[8] He L P, Hong X C, Dong J K, et al. Quantum transport evidence for the three-dimensional Dirac semimetal phase in Cd_3As_2. Phys Rev Lett, 2014, 113, 246402

[9] Liang T, Gibson Q, Ali M N, et al. Ultrahigh mobility and giant magnetoresistance in the Dirac semimetal Cd_3As_2. Nat Mater, 2015, 14, 280

[10] Zhao Y F, Liu H W, Zhang C L, et al. Anisotropic Fermi surface and quantum limit transport in high mobility three-dimensional Dirac semimetal Cd_3As_2. Phys Rev X, 2015, 5, 031037

[11] Jiang Z J, Zhao D, Jin Z, et al. Angular-dependent phase factor of Shubnikov-de Haas oscillations in the Dirac semimetal Cd_3As_2. Phys Rev Lett, 2015, 115, 226401

[12] Moll P J W, Nair N L, Helm T, et al. Transport evidence for Fermi-arc-mediated chirality transfer in the Dirac semimetal Cd_3As_2. Nature, 2016, 535, 366

[13] Zhang C, Narayan A, Lu S H, et al. Evolution of Weyl orbit and quantum Hall effect in Dirac semimetal Cd_3As_2. Nat Commun, 2017, 8, 1272

[14] Wang C M, Sun H P, Lu H Z, et al. 3D quantum Hall effect of Fermi arcs in topological semimetals. Phys Rev Lett, 2017, 119, 136806

[15] Uchida M, Nakazawa Y, Nishihaya S, et al. Quantum Hall states observed in thin films of Dirac semimetal Cd_3As_2. Nat Commun, 2017, 8, 2274

[16] Schumann T, Galletti L, Kealhofer D A, et al. Observation of the quantum Hall effect in confined films of the three-dimensional Dirac semimetal Cd_3As_2. Phys Rev Lett, 2018, 120, 016801

[17] Goyal M, Galletti L, Salmani-Rezaie S, et al. Thickness dependence of the quantum Hall effect in films of the three-dimensional Dirac semimetal Cd_3As_2. APL Mater, 2018, 6, 026105

[18] Zhang C, Zhang Y, Yuan X, et al. Quantum Hall effect based on Weyl orbits in Cd_3As_2. Nature, 2019, 331, 565

[19] Lin B C, Wang S, Wiedmann S, et al. Observation of an odd-integer quantum Hall effect from topological surface states in Cd_3As_2. Phys Rev Lett, 2019, 122, 036602

[20] Zhang Y, Zhang C, Gao H X, et al. Large Hall angle-driven magneto-transport phenomena in topological Dirac semimetal Cd_3As_2. Appl Phys Lett, 2018, 113, 072104

[21] Nishihaya S, Uchida M, Nakazawa Y, et al. Quantized surface transport in topological Dirac semimetal films. Nat Commun, 2019, 10, 2564

[22] Li C Z, Wang L X, Liu H W, et al. Giant negative magnetoresistance induced by the chiral anomaly in individual Cd_3As_2 nanowires. Nat Commun, 2015, 6, 10137

[23] Li H, He H T, Lu H Z, et al. Negative magnetoresistance in Dirac semimetal Cd_3As_2. Nat Commun, 2016, 7, 10301

[24] Aggarwal L, Gaurav A, Thakur G S, et al. Unconventional superconductivity at mesoscopic point contacts on the 3D Dirac semimetal Cd_3As_2. Nat Mater, 2016, 15, 32

[25] Wang H, Wang H C, Liu H W, et al. Observation of superconductivity induced by a point contact on 3D Dirac semimetal Cd_3As_2 crystals. Nat Mater, 2016, 15, 38

[26] Wang A Q, Li C Z, Li C, et al. 4π-periodic supercurrent from surface states in Cd_3As_2 nanowire-based Josephson junctions. Phys Rev Lett, 2018, 121, 237701

[27] Huang C, Zhou B T, Zhang H Q, et al. Proximity-induced surface superconductivity in Dirac semimetal Cd_3As_2. Nat Commun, 2019, 10, 2217

[28] Wang L X, Li C Z, Yu D P, et al. Aharonov-Bohm oscillations in Dirac semimetal Cd_3As_2 nanowires. Nat Commun, 2016, 7, 10769

[29] Wang L X, Wang S, Li J G, et al. Universal conductance fluctuation in Dirac semimetal Cd_3As_2 nanowires. Phys Rev B, 2016, 94, 161402

[30] Wang S, Lin B C, Zheng W Z, et al. Fano interference between bulk and surface states of a Dirac semimetal Cd_3As_2 nanowire. Phys Rev Lett, 2018, 120, 257701

[31] Zhou T, Zhang C, Zhang H S, et al. Enhanced thermoelectric proper-

ties of the Dirac semimeatl Cd_3As_2. Inorg Chem Front, 2016, 3, 1637

[32] Jia Z Z, Li C Z, Li X Q, et al. Thermoelectric signature of the chiral anomaly in Cd_3As_2. Nat Commun, 2016, 7, 13013

[33] Zhu C H, Wang F Q, Meng Y F, et al. A robust and tunable mid-infrared optical switch enabled by bulk Dirac fermions. Nat Commun, 2017, 8, 14111

[34] Wang Q S, Li C Z, Ge S F, et al. Ultrafast broadband photodetectors based on three-dimensional Dirac semimetal Cd_3As_2. Nano Lett, 2017, 17, 834

[35] Liu Y W, Zhang C, Yuan X, et al. Gate-tunable quantum oscillations in ambipolar Cd_3As_2 thin films. NPG Asia Mater, 2015, 7, e221

[36] Li C Z, Li J G, Wang L X, et al. Two-carrier transport induced Hall anomaly and large tunable magnetoresistance in Dirac semimetal Cd_3As_2 nanoplates. ACS Nano, 2016, 10, 6020

[37] Goyal M, Kim H, Schumann T, et al. Surface states of strained thin films of the Dirac semimetal Cd_3As_2. Phys Rev Mater, 2019, 3, 064204

[38] Jin H, Dai Y, Ma Y D, et al. The electronic and magnetic properties of transition-metal element doped three-dimensional topological Dirac semimetal Cd_3As_2. J Mater Chem C, 2015, 3, 3547

[39] Liu Y W, Tiwari R, Narayan A, et al. Cr doping induced negative transverse magnetoresistance in Cd_3As_2 thin films. Phys Rev B, 2018, 97, 085303

[40] Yuan X, Chen P H, Zhang L Q, et al. Direct observation of landau level resonance and mass generation in Dirac semimetal Cd_3As_2 thin films. Nano Lett, 2017, 17, 2211

[41] Sun Y, Meng Y F, Dai R H, et al. Slowing down photocarrier relaxation in Dirac semimetal Cd_3As_2 via Mn doping. Opt Lett, 2019, 44, 4103

[42] Zakhvalinskii V S, Nikulicheva T B, Lahderanta E, et al. Anomalous cyclotron mass dependence on the magnetic field and Berry's phase in $(Cd_{1-x-y}Zn_xMn_y)_3As_2$ solid solutions. J Phys Condens Matter, 2017, 29, 455701

[43] Schumann T, Goyal M, Kim H, et al. Molecular beam epitaxy of Cd_3As_2 on a III–V substrate. APL Mater, 2016, 4, 126110

[44] Nakazawa Y, Uchida M, Nishihaya S, et al. Molecular beam epitaxy of three-dimensionally thick Dirac semimetal Cd_3As_2 films. APL Mater, 2019, 7, 071109

[45] Kealhofer D A, Kim H, Schumann T. Basal-plane growth of cadmium arsenide by molecular beam epitaxy. Phys Rev Mater, 2019, 3, 031201

[46] Wang H L, Ma J L, Yu X Z, et al. Electric-field assisted switching of magnetization in perpendicularly magnetized (Ga,Mn)As films at high temperatures. J Phys D, 2017, 50, 025003

[47] Wang H L, Ma J L, Zhao J H. Giant modulation of magnetism in (Ga,Mn)As ultrathin films via electric field. J Semicond, 2019, 40, 092501